Improved detectivity of uncooled $InAs_{0.06}Sb_{0.94}$ photoconductors with long wavelength

Y. Z. GAO[a*], X. Y. GONG[a], G. H. WU[b], Y. B. FENG[b], T. KOYAMA[c], Y. HAYAKAWA[c]
[a]*College of Electronics and Information Engineering, Tongji University, Shanghai 201804, China*
[b]*Huaxing Infrared Device Company, Xian 712099, China*
[c]*Research Institute of Electronics, Shizuoka University, Johoku 3-5-1, Hamamatsu, Shizuoka 432-8011, Japan*

Uncooled $InAs_{0.06}Sb_{0.94}$ and $InAs_{0.02}Sb_{0.98}$ photoconductors with long wavelength were experimentally validated. Ge immersion lenses were set on the photoconductors. The detectors were fabricated using InAsSb epitaxial single crystals grown on InAs substrates by melt epitaxy (ME) technique. At room temperature, the spectral photoresponse showed that the peak detectivity $D_{\lambda p}$*at the wavelength of 6.5 μm reaches ≥ 5.0×10^9 cm $Hz^{1/2}$ W^{-1}, indicating the high sensitivity of the photoconductors. The detectivity D*of $InAs_{0.06}Sb_{0.94}$ detectors is 1.3×10^9 and 2.8×10^8 cm $Hz^{1/2}$ W^{-1} at the wavelength of 8 and 9 μm respectively, which is one order of magnitude higher than that of $InAs_{0.02}Sb_{0.98}$ detectors. The improvement of the sensitivity at 8 and 9 μm profits from the more arsenic composition in $InAs_{0.06}Sb_{0.94}$ epilayers.

(Received April 1, 2014; accepted November 13, 2014)

Keywords: InAsSb, Narrow bandgap, Single crystal, Spectral photoresponse

1. Introduction

The infrared (IR) detectors operated in 8-12 μm wavelength range have many applications, such as remote sensing, resource detection, environment monitoring and medical diagnosis. HgCdTe detector is the dominant system in this waveband at present. However, it suffers from chemical instability and nonuniformity due to the high Hg vapor pressure during its growth. InAsSb alloys with long wavelength have high electron and hole mobilities, good chemical stability and mechanical strength and hopeful performances operating at room temperature. It is very attractive to study InAsSb as a promising material alternative to HgCdTe [1, 2, 3]. However, the lattice mismatch between InAsSb epilayers and the binary compound substrates is rather large (for InAs is larger than 6%, for GaAs is 7.2 ~ 14.6%). Therefore it is a difficult task to grow long wavelength InAsSb single crystals with high quality. In our previous papers [4-9], thick InAsSb epilayers with cutoff wavelengths longer than 8 μm were grown on InAs and GaAs substrates by melt epitaxy (ME) method. The thicknesses of the epilayers reach several decade –100 μm. This thickness effectively suppresses the affection of the lattice mismatch resulting in a low dislocation density (the order of 10^4 cm^{-2}) in the epilayers.

In this work, high sensitivity uncooled $InAs_{0.06}Sb_{0.94}$ photoconductors with long wavelength were fabricated. The photoconductors are made from InAsSb epilayers with the thickness of 50 μm grown on InAs substrates by ME technology. Ge immersion lenses were set on the detectors. At room temperature, the peak detectivity $D_{\lambda p}$*at the wavelength of 6.5 μm is 5.6×10^9 cm $Hz^{1/2}$ W^{-1}. The detectivity D*at the wavelength of 8 μm is 1.3×10^9 cm $Hz^{1/2}$ W^{-1}, and 2.8×10^8 cm $Hz^{1/2}$ W^{-1} at 9 μm respectively. The detectivity of $InAs_{0.06}Sb_{0.94}$ detectors at 8 and 9 μm was improved one order of magnitude comparing with that of $InAs_{0.02}Sb_{0.98}$ detectors.

2. Experimental

InAsSb epilayers were grown on (100)-oriented n-InAs substrates in a horizontal LPE growth system in the high purity hydrogen ambient. The source materials were 7N Sb, In and non-doped InAs single crystals. The detailed growth process of ME method has been provided in the previous paper [7]. The key point is as follows: at the growth temperature (about 500°C), the melt is pushed to contact with the substrate, and the excess growth melt is immediately removed away from the substrate by pushing the melt holder. It is important that some melt is remained on the surface of the substrate at the growth temperature. Then the substrate was pushed under the flat part (the block) of the melt holder and cooled with a cooling rate of 0.5°C/min to obtain an epilayer. After the growth, the surfaces of the samples were polished by Al_2O_3 powder to achieve mirror smooth. X-ray diffraction (XRD) measurements for the samples were performed using an x-ray diffractometer (Rigaku D/MAX-2200PC, Cu barn) at a voltage of 40 kV and a

current of 40 mA. The composition distributions of the epilayers were measured by electron probe microanalysis (EPMA, JEOL JXA-8530F) at a voltage of 20 kV.

The immersion photoconductors were fabricated based on thick $InAs_{0.06}Sb_{0.94}$ and $InAs_{0.02}Sb_{0.98}$ epilayers grown by ME. InAs substrates were entirely removed away during the device process. Ge optical lenses were set on the photoconductors. The area of the sensitive elements is 0.05 × 0.05 cm^2. Indium is employed as the electrode. There are no passivation and antireflective coatings deposited on the surfaces of the elements and lenses. The spectral photoresponse of InAsSb photoconductors were measured by a Fourier transform infrared (FTIR) spectrometer, and the absolute responsivity was calibrated by a standard blackbody source at a temperature of 500 K and a modulation frequency of 1200 Hz. The applied bias current on the detectors was 10 mA.

3. Results and discussion

3.1. Structural characterization

Structural characterization of the samples is measured using high-resolution x-ray diffraction. Fig. 1 shows XRD curves of an InAs/$InAs_{0.06}Sb_{0.94}$ sample.

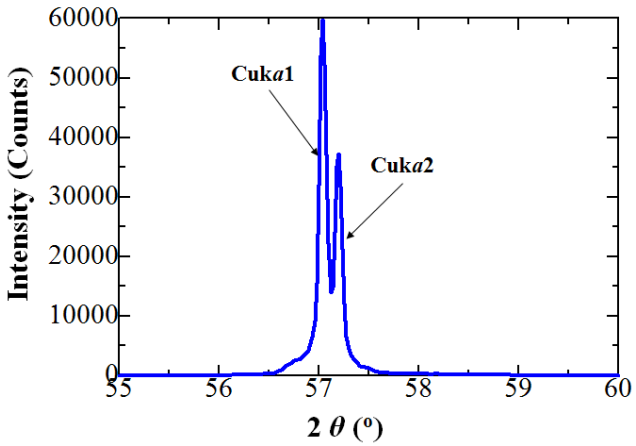

Fig. 1. XRD curves of an InAs/$InAs_{0.06}Sb_{0.94}$ sample. The lattice mismatch between the epilayer and substrate is estimated to be 6.52%.

In Fig. 1, (400) Cukα1 and Cukα2 diffraction peaks of InAsSb epilayers clearly appear, and no other crystal structures are observed. The growth direction of the epilayers agrees with the surface direction of InAs substrates, i.e. the (100) orientation. This demonstrates that InAsSb epilayers are indeed single crystals. The sharpness and the full-width at half-maximum (FWHM) of 360 arcsec of the InAsSb (400) Cukα1 diffraction peak indicate the high quality of the epilayers. According to the Bragg diffraction equation, the lattice constant for $InAs_xSb_{1-x}$ samples shown in Fig. 1 is estimated to be 6.4533 Å. Based on the Vegard Law [10], the arsenic mole fraction in the epilayers can be calculated as

$$x = (a_{InAsSb} - a_{InSb})/(a_{InAs} - a_{InSb}) \qquad (1)$$

where x is the arsenic mole fraction in the epilayers, and a is the lattice constant. The arsenic mole fraction is calculated to be 0.06 for the samples in Fig. 1. The arsenic atomic fraction in the epilayer measured by EPMA is 6.2%, which is in agreement with that obtained by XRD measurements. The lattice constant of $InAs_{0.06}Sb_{0.94}$ samples is smaller than that of InSb (6.4789 Å). It indicates the lattice compression of InAsSb crystals grown by ME due to arsenic atoms substitution in the lattice. $InAs_{0.06}Sb_{0.94}$ single crystals with good quality have been grown by ME under the lattice mismatch of 6.52% between the epilayers and InAs substrates.

The dependence of the bandgap E_g on the composition for $InAs_xSb_{1-x}$ alloys can be expressed as [11]

$$E_g(x) = 0.434 - 0.771(1-x) + 0.59(1-x)^2 - 2.8\times10^{-4}T \qquad (2)$$

This formula predicts that E_g (x = 0.06) = 0.1466 eV and E_g (x = 0.02) = 0.1611 eV at T = 300 K.

3.2. Composition distribution

Fig. 2 (a) – (c) exhibit EPMA composition distribution images of Sb, As and In in the cross section of an InAs/$InAs_{0.06}Sb_{0.94}$ sample respectively. Fig. 2 (a) shows that Sb is concentrated in the $InAs_{0.06}Sb_{0.94}$ epilayer, and the distribution of Sb in the epilayer is comparatively uniform. In Fig. 2 (a), the red dots in the substrate are the noise dots of EPMA measurement, i.e., Sb is not existed in the InAs substrate. As seen in Fig. 2 (b) that the distribution of As in the InAs substrate is evidently more than that in the epilayer, because the arsenic atomic fraction in the epilayer is only 6.2%. Fig. 2 (c) shows that the distribution tendency of In in the sample does not obviously vary since In contains both in the epilayer and substrate.

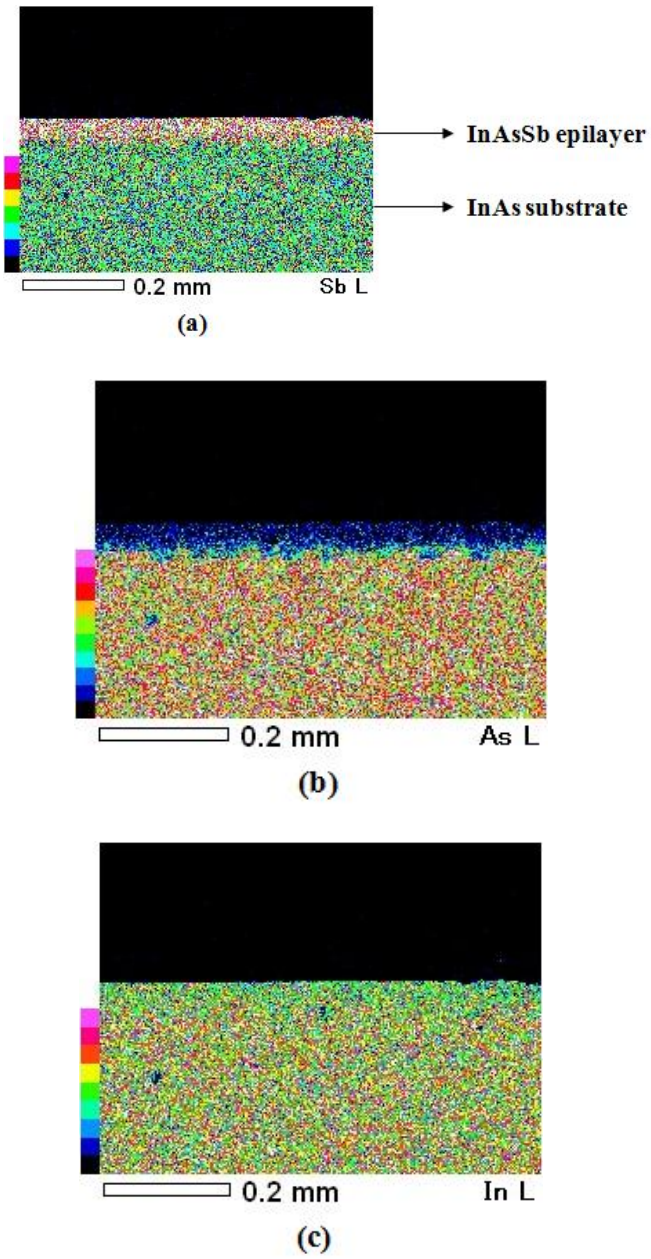

Fig. 2. Distribution images of Sb (a), As (b) and In (c) in the cross section of an InAs/$InAs_{0.06}Sb_{0.94}$ sample measured by EPMA.

3.3. Uncooled spectral photoresponse

Fig. 3 shows the spectral photoresponse of InAsSb photoconductors at room temperature, and immersed germanium lenses were set on the detectors. In Fig. 3, $InAs_{0.06}Sb_{0.94}$ and $InAs_{0.02}Sb_{0.98}$ detectors are labeled by a and b respectively. The cutoff wavelength of a detector is usually defined as the wavelength at 10% of the peak response. The cutoff wavelength of sample a and b is 8.4 and 7.5 μm in Fig. 3 respectively. The bandgap of 0.1476 and 0.1653 eV for $InAs_{0.06}Sb_{0.94}$ and $InAs_{0.02}Sb_{0.98}$ detectors obtained in Fig. 3 is in agreement with that of 0.1466 and 0.1611 eV calculated by Equation (2). They are narrower than that of InSb (0.17 eV). The bandgap narrowing of InAsSb materials grown by ME is mainly attributed to the lattice contraction due to the incorporation of arsenic in the lattice. The lattice constant of the $InAs_{0.06}Sb_{0.94}$ epilayer (6.4533 Å) is smaller than that of the $InAs_{0.02}Sb_{0.98}$ epilayer (6.4692 Å). The smaller lattice constant of the $InAs_{0.06}Sb_{0.94}$ epilayer resulting in the narrower bandgap and longer cutoff wavelength of the detector (sample a). Additionally, the non-regular arrangement of atoms in the lattice may also affect the energy band bowing for Ⅲ-Ⅴ mixed crystals.

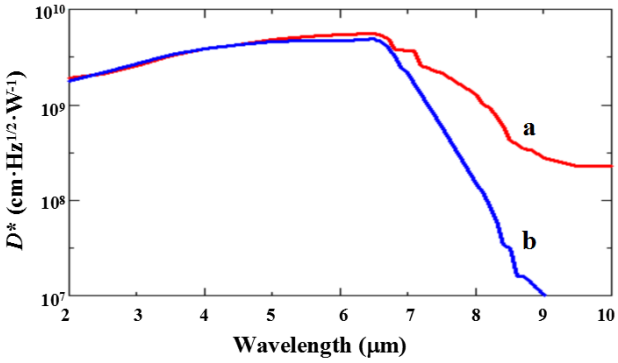

Fig. 3. Uncooled Spectral photoresponse of an $InAs_{0.06}Sb_{0.94}$ photoconductor labeled by a and an $InAs_{0.02}Sb_{0.98}$ photoconductor labeled by b. Ge immersion lenses were set on the photoconductors.

At room temperature, the peak detectivity $D_{\lambda p}$* (6.5 μm, 1200 Hz) at the wavelength of 6.5 μm is 5.6×10^9 and 5.0×10^9 cm $Hz^{1/2}$ W^{-1} for sample a and b respectively. It indicates the high sensitivity of long wavelength InAsSb detectors. As shown in Fig. 3, the detectivity D* at the wavelength of 8 μm of sample a is 1.3×10^9 cm $Hz^{1/2}$ W^{-1}, and that of sample b is 1.5×10^8 cm $Hz^{1/2}$ W^{-1}. D* at the wavelength of 9 μm for sample a and b is 2.8×10^8 and 1.0×10^7 cm $Hz^{1/2}$ W^{-1} respectively. The detectivity at 8 and 9 μm of $InAs_{0.06}Sb_{0.94}$ detectors is nearly one order of magnitude higher than that of $InAs_{0.02}Sb_{0.98}$ detectors, which is due to the more arsenic composition in $InAs_{0.06}Sb_{0.94}$ epilayers.

Uncooled $InAs_{0.06}Sb_{0.94}$ detectors with long wavelength have the good performances. This is benefit from the following reasons: (1) Ge immersion lenses were set on the photoconductors. The incident IR radiation was focused by the lenses, thus the radiation energy density on the photosensitive surfaces was raised. The immersion lens is able to increase the signal-to-noise ratio and detectivity of the detectors about one order of magnitude. (2) $InAs_{0.06}Sb_{0.94}$ epilayers with the thickness of 50 μm grown by ME are single crystals with device-level quality. The thick epilayers have the properties of bulk crystals. The intrinsic semiconductors are suitable for fabricating uncooled photodetectors,

since the high density of states in the valence and conduction bands of them gives rise to the strong absorption of IR radiation [12].

4. Conclusions

Uncooled $InAs_{0.06}Sb_{0.94}$ and $InAs_{0.02}Sb_{0.98}$ photoconductors with Ge immersion lenses were successfully fabricated. The photoconductors were based on thick InAsSb epilayers grown on InAs substrates by ME. XRD spectra and EPMA composition distribution images showed that the epilyers are single crystals with good quality and homogeneity. A fundamental agreement of the bandgap between the experimental spectral photoresponse and theoretical calculation is obtained indicating the bandgap narrowing of this material. At room temperature, the peak detectivity was 5.6×10^9 cm $Hz^{1/2} W^{-1}$ at the wavelength of 6.5 μm, and the detectivity was 1.3×10^9 and 2.8×10^8 cm $Hz^{1/2} W^{-1}$ at 8 and 9 μm for $InAs_{0.06}Sb_{0.94}$ immersion detectors respectively. The measurement results of the detectors indicate the high performance and possible applications for IR detection and imaging.

Acknowledgements

The authors acknowledge the financial assistance provided by the Fundamental Research Funds for the Central Universities in China.

References

[1] D. Lackner, M. Steger, M. L. W. Thewalt, O. J. Pitts, Y. T. Cherng, S. P. Watkins, E. Plis, S. Krishna, J. Appl. Phys. **111**, 034507 (2012).
[2] E. H. Steenbergen, Y. Huang, J. ‐H. Ryou, L. Ouyang, J. ‐J. Li, D. J. Smith, R. D. Dupuis, Y. ‐H. Zhang, Appl. Phys. Lett. **99**, 071111 (2011).
[3] V. K. Dixit, B. Bansal, V. Venkataraman, H. L. Bhat, K. S. Chandrasekharan, B. M. Arora, J. Appl. Phys. **96**, 4989 (2004).
[4] Y. Z. Gao, X. Y. Gong, H. Kan, M. Aoyama, T. Yamaguchi, Jpn. J. Appl. Phys. **38**, 1939 (1999).
[5] Y. Z. Gao, H. Kan, M. Aoyama, T. Yamaguchi, Jpn. J. Appl. Phys. **39**, 2520 (2000).
[6] Y. Gao, H. Kan, T. Yamaguchi, Cryst. Res. Technol. **35**, 943 (2000).
[7] Y. Z. Gao, H. Kan, F. S. Gao, X. Y. Gong, T. Yamaguchi, J. Cryst. Growth. **234**, 85 (2002).
[8] Y. Z. Gao, X. Y. Gong, Y. H. Chen, T. Yamaguchi, Proc. of SPIE. **6029**, 60291l (2005).
[9] Y. Z. Gao, X. Y. Gong, W. Z. Fang, G. H. Wu, Y. B. Feng, Jpn. J. Appl. Phys. **48**, 080202 (2009).
[10] A. R. Denton, N. W. Ashcroft, Phys. Rev. A. **43**, 3161 (1991).
[11] H. H. Wieder, A. R. Clawson, Thin Solid Films. **15**, 217 (1973).
[12] J. Piotrowski, A. Rogalski, Infrared Phys. Technol. **46**, 115 (2004).

*Corresponding author: gaoyuzhu@tongji.edu.cn